7.1. Introduction

As discussed in Chapter 1, the virgin samples of $LaMnO_3$ manganite display an A-type antiferromagnetic (AFM) with insulating nature [Ritter et al. (1997)]. On doping of divalent cations like Ca^{2+}, Ba^{2+} or Sr^{2+} at La^{3+} site parent compound converts into mixed valence state of Mn^{4+} & Mn^{3+} leading to double exchange (DE) interactions between Mn^{3+} ($t^3_{2g}e^1_g$, S = 2) and Mn^{4+} ($t^3_{2g}e^0_g$, S = 3/2) cations via O^{2-} anion due to hopping of electrons from e_g (Mn^{3+}) to t_{2g} (Mn^{4+}) resulting ferromagnetic (FM) ordering of Mn moments [Markovich et al. (2010); Gasmi et al. (2009); Hintze et al. (2017)]. In the mixed-valence manganites with composition range $0.2 \leq x \leq 0.4$, the ferromagnetism due to DE interaction dominates over the other interactions [Gayathri et al. (1997)]. The DE interactions also depend on the ratio of Mn^{3+} to Mn^{4+} ions, so by tuning the ratio of Mn^{3+}/Mn^{4+} one can tune FM nature of the system directly. The $LaMnO_3$ manganite doped with Barium received very less attention as compared to the manganites doped with Calcium and Strontium, even though its T_C is above room temperature for wide composition range. The CMR applications of any system require FM Curie temperature T_C near to room temperature (RT). The requirement of T_C near RT (for the magnetic system having T_C above RT) can be achieved by an appropriate replacement at Mn-site by a non-magnetic ion as a result of weakening in DE interactions and lowering in the value of T_C. It should also enhance non-metallic nature i.e. increased resistivity which causes improvement in magneto-resistive (MR) properties [Zhu et al. (2006); Hu et al. (2002)]. Since, $La_{0.6}Ba_{0.4}MnO_3$ manganite has the value of T_C well above RT (T_C ~ 335 K), by doping with a non-magnetic ion such as Ti^{4+} one can bring T_C near to RT [Hazzez et al. (2016)]. Keeping these factors in mind, we have investigated $La_{0.6}Ba_{0.4}Mn_{1-x}Ti_xO_3$ perovskite manganites system and the results will be presented in this chapter. The replacement of isovalent cation is expected to be

more remarkable because it should not affect the crystallographic nature of the parent systems due to the slight difference in the ionic radii of tetravalent Ti^{4+} (0.605 Å) and Mn^{4+} (0.53 Å). However, it should robustly influence the DE stimulated FM ordering of the virgin compound $La_{0.6}Ba_{0.4}MnO_3$ due to the existence of non-magnetic Ti^{4+} cation. Certainly, this is what generally observed for the B-site substituted manganites with a composition close to $La_{0.67}A_{0.33}BO_3$ (A = Ba, Sr and B = Mn, Ti) [Gasmi et al. (2009); Hu et al. (2002)].

In this chapter, we will present the effect of substitution of non-magnetic Ti^{4+} ions at Mn-site on the structural and magnetic behaviour of $La_{0.6}Ba_{0.4}Mn_{1-x}Ti_xO_3$ ($0.02 \leq x \leq 0.08$). Structural analysis by the Rietveld structure refinement using X-ray diffraction patterns of the synthesized samples shows that $La_{0.6}Ba_{0.4}Mn_{1-x}Ti_xO_3$ crystallizes into cubic Pm-3m symmetry. However magnetic characterization of the samples reveals reduction in T_C of $La_{0.6}Ba_{0.4}Mn_{1-x}Ti_xO_3$ with increasing Ti-doping concentration consistent with the predictions of molecular field theory of the dilution of a magnetic lattice. Appearance of the Griffiths Phase for the sample with x = 0.08 is observed. Coupling between spin and orbital moments in $La_{0.6}Ba_{0.4}Mn_{1-x}Ti_xO_3$ perovskite manganites is shown at lower temperatures.

7.2. Experimental Details

The polycrystalline samples of Ti-doped $La_{0.6}Ba_{0.4}Mn_{1-x}Ti_xO_3$ ($0.02 \leq x \leq 0.08$) manganites were prepared by the glycine-nitrate combustion method and then calcined at 1300^oC for 6 hrs [Kumar et al. (2019)]. The details of the synthesis process are summarized in Chapter 2. In this chapter $La_{0.6}Ba_{0.4}Mn_{1-x}Ti_xO_3$ is denoted by LBMTO. The synthesized samples were characterized by powder X-ray diffraction (XRD), scanning electron spectroscopy (SEM) equipped with energy dispersive X-ray spectroscopy (EDS) facilities and magnetization measurements as a function of

temperature and magnetic field. The temperature dependent magnetizations were recorded in the temperature range 2-390 K. The magnetic field dependent magnetizations were measured at 10 and 300 K in the magnetic field range -60 kOe to +60 kOe. Temperature and frequency dependent ac susceptibility measurement were done in the temperature range 2-390 K at 100, 300 and 500 Hz.

7.3. Results and Discussion

7.3.1. Microstructural and Elemental Analysis

Fig. 7.1 shows SEM micrographs of the powder samples of LBMTO manganites with x = 0.02, 0.04, 0.06 and 0.08. The average particles/grains sizes were estimated by the help of ImageJ software. In the process of calculation of average particle size, we considered maximum number of particles in the calculation. The calculated average particle size was found to be 695, 720, 845 and 970 nm for x = 0.02, 0.04, 0.06 and 0.08, respectively. The analysis of the SEM micrographs reveals that particle size increases with increasing doping concentration of Ti-ions in $La_{0.6}Ba_{0.4}MnO_3$ manganite at Mn-site. Thus the substitution of Ti- is enhancing the grain growth.

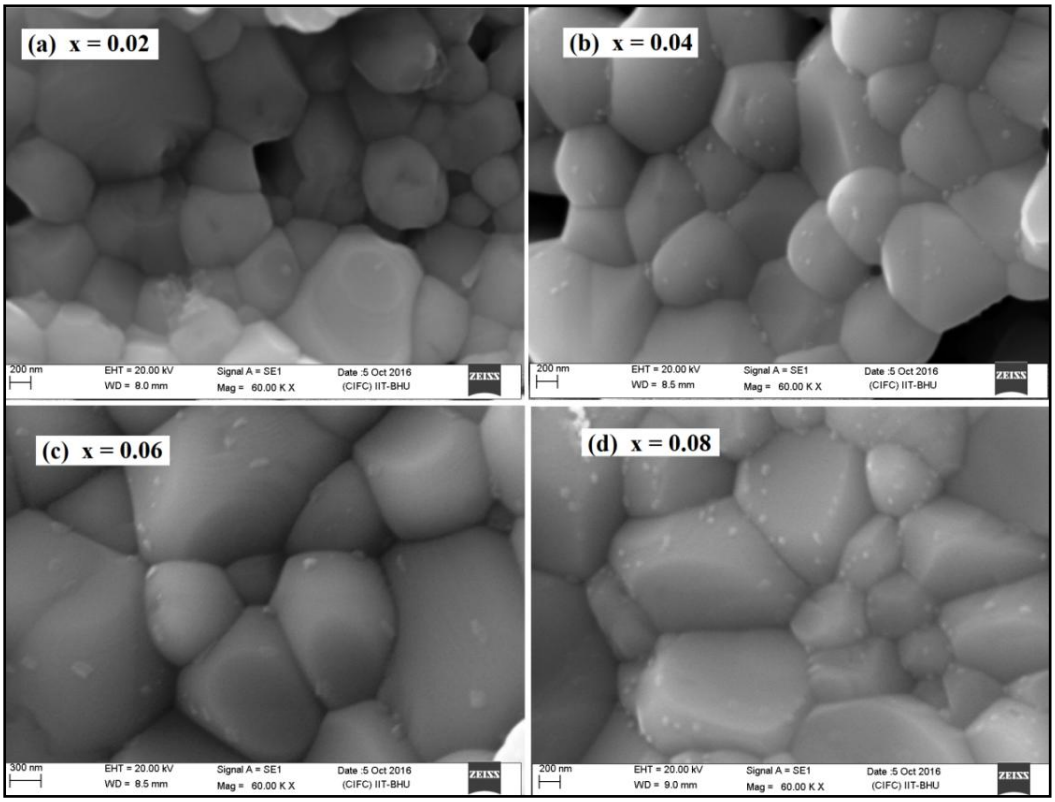

Figure 7.1: The SEM micrographs for $La_{0.6}Ba_{0.4}Mn_{1-x}Ti_xO_3$ manganites with x = (a) 0.02, (b) 0.04, (c) 0.06 and (d) 0.08.

Figs. 7.2(a-d) display EDS spectra for LBMTO manganites with compositions x = 0.02, 0.04, 0.06 and 0.08, respectively. The characteristic peaks of La, Ba, Mn, Ti and O present in the EDS spectra reveal the presence of constituent chemical elements in the studied samples. The qualitative behavior of the EDS spectra is similar for all samples. We also performed quantitative analysis of the EDS spectra by quantifying atomic percentages of the constituent atoms. The quantitative analysis was performed by excluding lighter element "oxygen" in our calculations, because this technique is not suitable for the detection of lighter element. Since the doping concentration of Ti^{4+} ions at the Mn-site is very small. So, there may be some fluctuations in the atomic percentage. The theoretical and experimental atomic percentages for La, Ba, Mn and Ti

are given in **Table 7.1**, which shows that the atomic percentage of Ti increases with increasing doping concentration of Ti^{4+} ions.

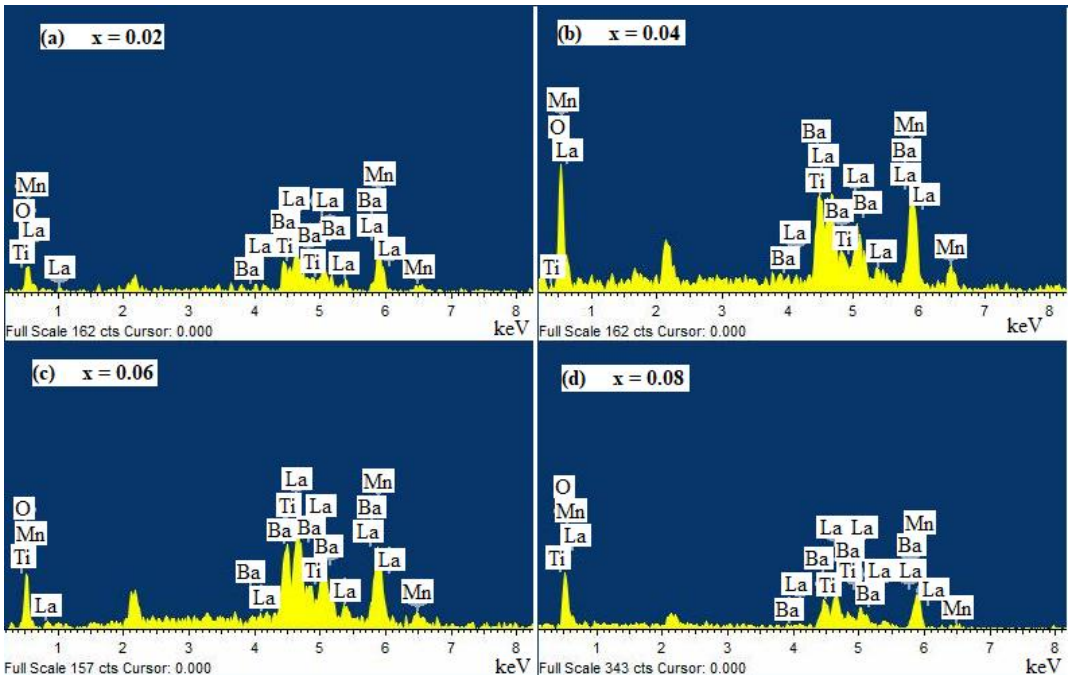

Figure 7.2: Electron Dispersive X-ray spectroscopy (EDS) spectrum for $La_{0.6}Ba_{0.4}Mn_{1-x}Ti_xO_3$ manganites with x = (a) 0.02, (b) 0.04, (c) 0.06 and (d) 0.08.

Table 7.1: Experimentally observed and theoretically calculated atomic percentages for the La, Ba, Mn and Ti atoms present in $La_{0.6}Ba_{0.4}Mn_{1-x}Ti_xO_3$ ($0.02 \leq x \leq 0.08$) manganites obtained from EDS measurements.

x	La		Ba		Mn		Ti	
	Theo.	**Exp.**	**Theo.**	**Exp.**	**Theo.**	**Exp.**	**Theo.**	**Exp.**
0.02	30.00	26.17	20.00	16.50	49.00	55.20	1.00	2.13
0.04	30.00	33.89	20.00	23.11	48.00	48.82	2.00	3.18
0.06	30.00	31.23	20.00	21.18	47.00	43.30	3.00	4.29
0.08	30.00	29.15	20.00	18.18	46.00	46.02	4.00	5.69

7.3.2. Crystal Structure: Rietveld Refinement

The room temperature XRD patterns for polycrystalline LBMTO manganites with nominal compositions (x = 0.02, 0.04, 0.06 and 0.08) are displayed in **Fig. 7.3**(a). All the reflections in the XRD patterns correspond to ideal cubic perovskite structure with $Pm\bar{3}m$ space group as all the diffraction profiles are singlet. No, any additional secondary impurity phase was detected in the XRD patterns confirming the formation of phase pure samples. **Fig. 7.3**(b) shows zoomed XRD peak corresponding to (110) reflection for all the samples, which is shifting towards lower angle sides with increasing Ti-doping contents showing enhancement in the lattice parameter and unit cell volume. The Rietveld structure refinement confirms that lattice parameter and unit cell volume increase with increasing doping concentration of Ti^{4+}-ions. **Fig. 7.3**(c) shows variation of lattice constant "a" and unit cell volume "V" with Ti-doping concentration at Mn-site. The scattered data points indicate values obtained from refinement, while continuous line shows theoretically fitted curve with exponential function. The refined lattice constant "a" increases exponentially with increasing doping concentration of Ti^{4+}-ions at Mn-site according to the equation: $a = a_0 - a_1 \times e^{-x/t}$, where a_0, a_1 and t are fitting parameters and are found to be a_0 = 3.91769(5) Å, a_2 = 0.01158(9) Å and t = 0.029(5). The lattice constant "a" increases from 3.91182(5) Å for x = 0.02 to 3.91701(4) Å for x = 0.08, while unit cell volume "V" increases from 59.860(1) $Å^3$ for x = 0.02 to 60.099(1) $Å^3$ for x = 0.08 exponentially following the equation: $V = V_0 - V_1 \times e^{-x/t}$, where, V_0 = 60.13(2) $Å^3$, V_1= 0.53(4) $Å^3$ and t = 0.029(5). Refined lattice parameters, unit cell volume, Mn-O, La-O bond lengths and particle sizes for various compositions are listed in **Table 7.2**.

Table 7.2: Particle size, lattice parameter, unit cell volume, bond-lengths (d_{Mn-O} and d_{La-O}) and χ^2 for LBMTO manganites with x = 0.02, 0.04, 0.06 and 0.08 for $Pm\bar{3}m$ space group.

Sample	d (nm)	a = b = c (Å)	V (Å^3)	d_{Mn-O} (Å)	d_{La-O} (Å)	χ^2
x = 0.02	695	3.91182(5)	59.860(1)	1.95591(0)	2.76607(3)	1.762
x = 0.04	720	3.91482(4)	59.998(1)	1.95741(1)	2.76819(3)	1.650
x = 0.06	845	3.91605(4)	60.055(1)	1.95802(1)	2.76906(3)	1.892
x = 0.08	970	3.91701(4)	60.099(1)	1.95851(3)	2.76974(3)	1.851

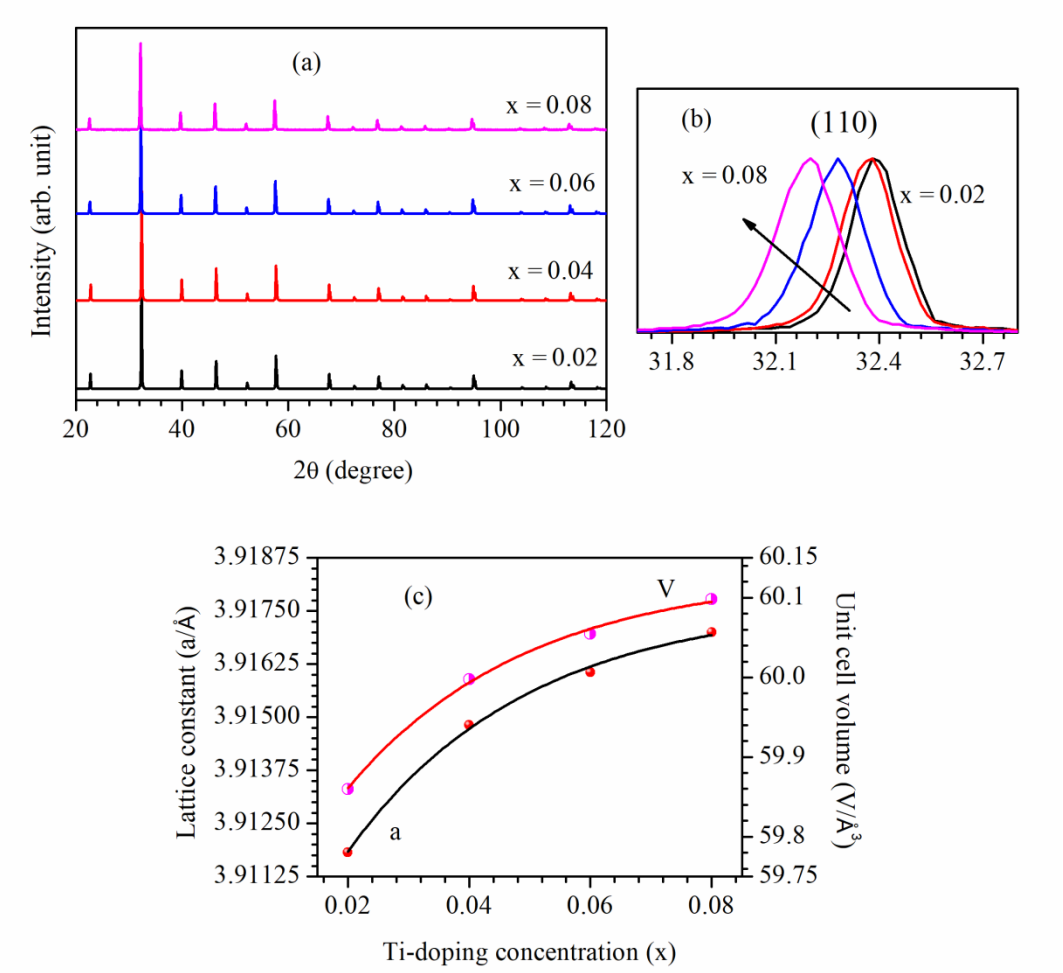

Figure 7.3: (a) RT X-ray diffraction patterns, (b) Bragg's reflection (110) for LBMTO manganites with x = 0.02, 0.04, 0.06 and 0.08 and (c) Variation of lattice constant and unit cell volume as a function of Ti-doping concentration (x).

In the process of Rietveld structure refinement, we have chosen substitution of Ti^{4+}-ions at Mn-site in the LBMTO manganites systems. The Rietveld refinement of the XRD patterns was performed by considering cubic crystal structure having $Pm\bar{3}m$ space group, in which La^{3+}/Ba^{2+} ions occupy 1(a) sites at (1/2, 1/2, 1/2), $Mn^{3+}/Mn^{4+}/Ti^{4+}$ ions engage 1(b) sites at (0, 0, 0) and O^{2-} ions occupy 3(c) sites at (1/2, 0, 0) [Latif (2012)]. The Rietveld fits for LBMTO manganites are shown in **Fig. 7.4**, display a very good fit between observed and simulated XRD patterns. The observed XRD pattern is shown by scattered plot while calculated pattern is shown by continuous curve overlapping on the observed data. The lower continuous curve indicates difference pattern between observed and calculated XRD patterns. The vertical bars indicate positions of the Bragg's peaks. After completing Rietveld analysis, we also estimated bond lengths between Mn and O (d_{Mn-O}) and La and O (d_{La-O}), which increases with increasing Ti^{4+}-ions concentration. This suggests that smaller Mn^{4+} ions are being substituted by the larger Ti^{4+} ions. **Fig. 7.5** shows MnO_6 octahedra for LBMTO manganites with x = 0.02 and 0.08 showing bond-length Mn-O. The MnO_6 octahedral was drawn by using crystallographic information file (CIF file) obtained from Rietveld structure refinement with the help of VESTA software.

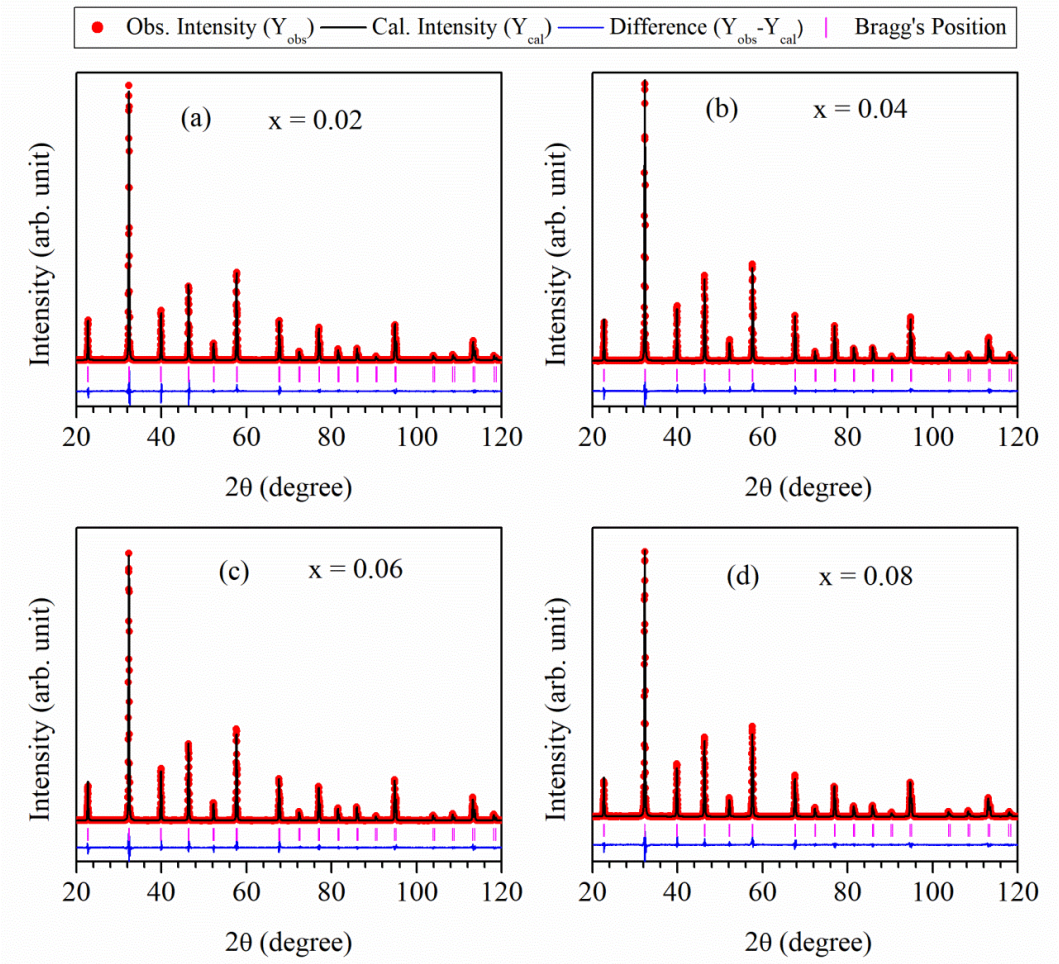

Figure 7.4: Rietveld fits for Ti-doped LBMTO manganites with (a) x = 0.02, (b) 0.04, (c) 0.06 and (d) 0.08.

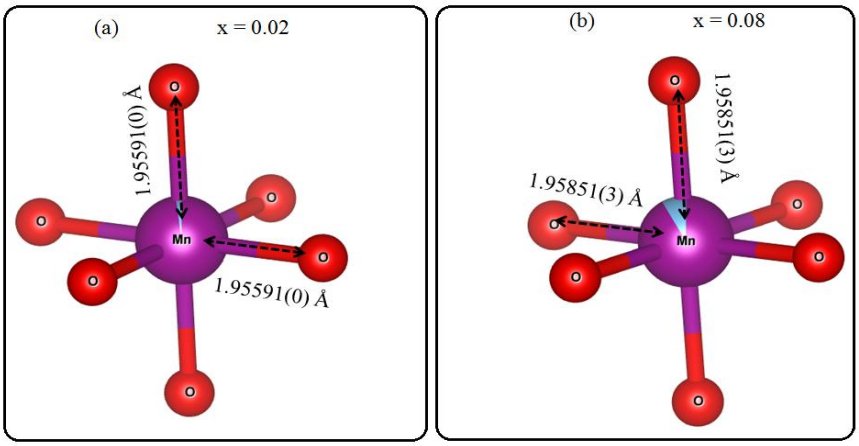

Figure 7.5: MnO_6 octahedra showing bond-length Mn-O for LBMTO manganites with (a) x = 0.02 and (b) x = 0.08.

7.3.3. Magnetic Properties

7.3.3.1. Temperature Dependent Magnetization Studies

The temperature dependence of the zero field cooled (M_{ZFC}) and field cooled (M_{FC}) magnetizations of LBMTO perovskites with x = 0.02, 0.04, 0.06 and 0.08 are shown in **Fig. 7.6**(a). The temperature dependence of magnetization M(T) were recorded at an applied field of 200 Oe in the temperature range 2-390 K. During the M_{ZFC} measurement the sample was cooled from 390 K to 2 K in the absence of magnetic field, and then the measuring field is applied for the measurement of magnetization from 2 to 390 K, while during M_{FC} measurement the sample was cooled first from 390 K to 2 K under the applied magnetic field and then the magnetization was recorded from 2 to 390 K in warming mode. From the first sight of the M(T) curves in low temperature region, one can see that magnetization M (in the unit of emu/gm) increases with doping of non-magnetic Ti^{4+}-ion. Generally the doping of non-magnetic ions on a magnetic site results decrease in magnetization when the concentration of doping ion is increased [Dayal et al. (2015); Zhu et al. (2006); Ho et al. (2016)]. The reason of this type of magnetization change is discussed in detail in the upcoming section. In the higher temperature region, the values of M_{FC} and M_{ZFC} are very close to zero (PM state) and increase slowly with decreasing temperature, but in the vicinity of phase transition magnetization increases suddenly and exhibits a broad hump (T_B). Below the broad hump M_{ZFC} decreases slowly, whereas, M_{FC} increases smoothly i.e., M_{FC} and M_{ZFC} show deviation between each other in low temperature region, which may be due to spin glass or spin glass clusters or superparamagnetic behavior of the samples discussed in the forthcoming section [Thanh et al. (2014)]. The irreversibility temperature T_{irr} defined as the temperature below which M_{FC} and M_{ZFC} just start deviating from each other. The irreversibility temperature decreases with increasing x

from 332 K for x = 0.02 to 242 K for x = 0.08. In **Fig. 7.6**(c), we have plotted irreversible magnetization $M_{irr} = M_{FC} - M_{ZFC}$ as a function of temperature for all the samples. The irreversible magnetization M_{irr} vanishes above T_{irr} and increases continuously below T_{irr} to low temperature, whereas, the M_{irr} curves for x = 0.02 and 0.04 exhibit a peak near T_C. A similar result was also observed in $Nd_{0.84}K_{0.12}MnO_3$ manganite [Samantaray et al. (2010)]. All the samples of LBMTO perovskite manganites exhibit a PM to FM phase transition at characteristic Curie temperature (T_C). The value of T_C was determined by the temperature corresponding to the minima appearing in the dM_{ZFC}/dT vs. T curves as shown in **Fig. 7.6**(b). The value of T_C decreases with the increasing doping concentration of Ti^{4+}-ion due to the weakening of DE interactions between Mn^{3+} and Mn^{4+} cations. **Fig. 7.6**(d) displays variation of T_C as a function of Ti-doping concentration (x), where, T_C reduces exponentially with Ti-doping concentration from 309 K for the sample with x = 0.02 to 212 K for x = 0.08. The experimental value of T_C was fitted using the exponential expression given by Equation (7.1):

$$T_C = T_0 - T_1 \times e^{x/t} \tag{7.1}$$

Here, T_0, T_1 and t are fitting parameters. The fitting parameters obtained from fitting are T_0 = 402.59 K, T_1 = 73.14 K and t = 0.08 [Kumar et al. (2019)]. Further, the reduction in the value of T_C also indicates that AFM ordering is increasing as the concentration of Ti^{4+}-ion is increased [Dayal et al. (2015)].

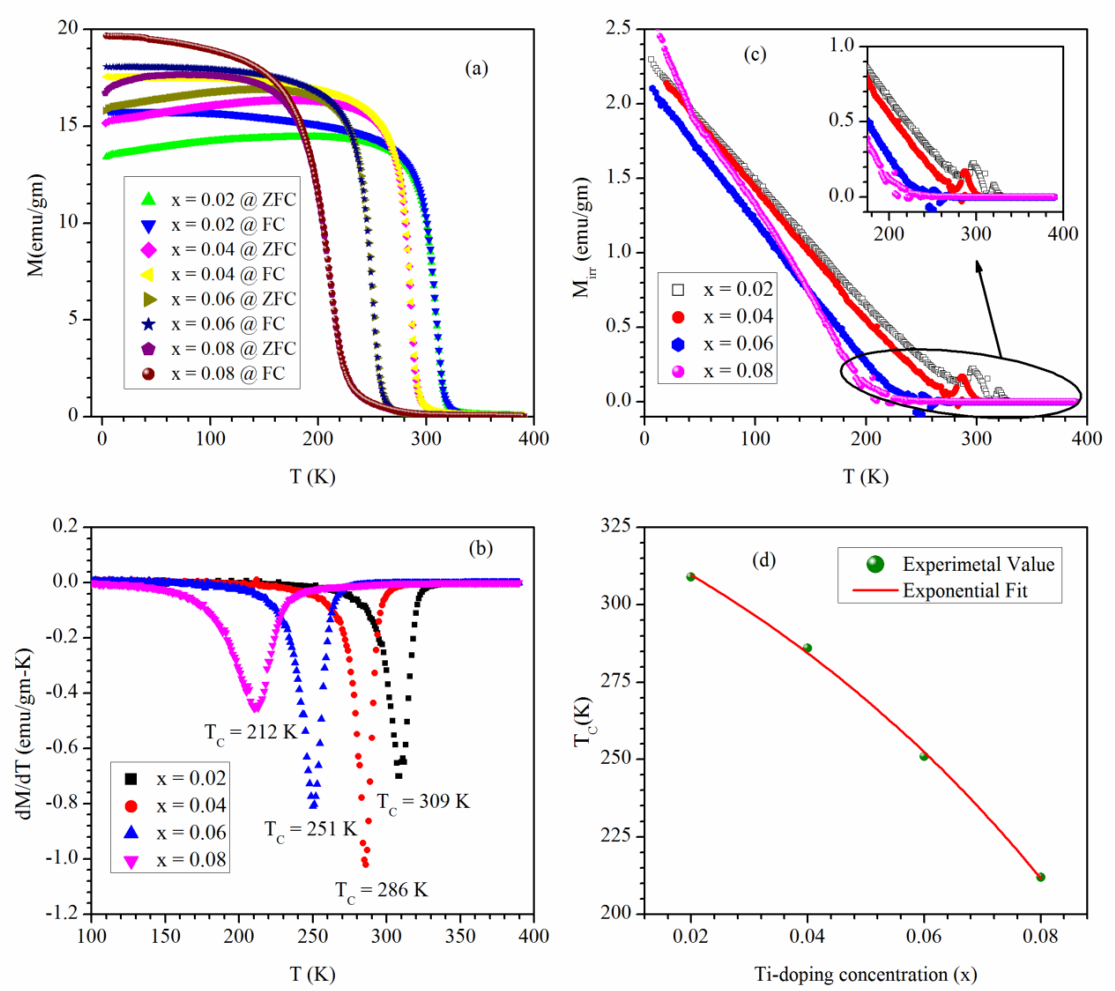

Figure 7.6: Temperature dependence of (a) ZFC and FC magnetizations curves, (b) irreversible magnetization and (c) dM/dT vs. T plots for LBMTO manganites with x = 0.02, 0.04, 0.06 and 0.08. (d) Variation in T_C as a function of Ti^{4+}-ion concentration.

7.3.3.2. Temperature Dependent Inverse Susceptibility Studies

Fig. 7.7(a) shows temperature dependence of inverse dc molar susceptibility for LBMTO manganites with x = 0.02, 0.04, 0.06 and 0.08. In higher temperature regime ($T > T_C$) inverse molar susceptibility follows Curie-Weiss law given by Equation (7.2):

$$\chi_m^{-1} = (T - \theta_{CW})/C \qquad (7.2)$$

Where, θ_{CW} is Curie-Weiss temperature and C is Curie constant. The value of θ_{CW} was calculated from the intercept of the straight line with the temperature axis and value of C was calculated from the inverse of the slope of straight line (C = 1/slope) in the higher

temperature region, respectively. The numerical value of θ_{CW} decreases linearly from 313.34 K for x = 0.02 to 245.65 K for x = 0.08 with doping of Ti^{4+}-ions at Mn-site. While, the value of C increases exponentially from 4.65 emu-K/Oe-mol for x = 0.02 to 5.31 emu-K/Oe-mol for x = 0.08, according to the relation: $C = C_0 - C_1 e^{-x/t}$, where C_0, C_1 and t are fitting parameters. The value of fitting parameters obtained after exponential fit are C_0 = 5.30(4) emu-K/Oe-mol, C_1 = 2.9(9) emu-K/Oe-mol and t = 0.013(3). The experimental effective PM moment in the unit of Bohr magneton (μ_B) was calculated using the Equation (7.3):

$$\mu_{eff}^{exp}(\mu_B) = \left(\frac{3Ck_B}{N_a \mu_B^2}\right)^{1/2} = \sqrt{8C} \tag{7.3}$$

Here, k_B is Boltzmann constant and N_a is Avogadro number. The value of $\mu_{eff}^{exp}(\mu_B)$ increases exponentially from 6.10 μ_B for x = 0.02 to 6.52 μ_B for x = 0.08, consistent with the manner of Curie constant (C) and inconsistent with the behavior of T_C. This unusual behavior of effective PM moment can be explained by using Zener pair of Mn^{3+}-Mn^{4+}, i.e., due to presence of short-range FM ordering in PM regime, which increases with increasing doping concentration of Ti^{4+}-ion. Appearance of FM ordering in PM regime may be due to double exchange interaction between Zener pair of Mn^{3+}-Mn^{4+} via O^{2-}, i.e. Mn^{3+} -O^{2-} -Mn^{4+}, which results Griffith's phase in the compound(s) with higher doping concentration of Ti^{4+}-ions. The value of theoretical effective PM moment $\mu_{eff}^{theo}(\mu_B)$ in the units of Bohr magneton (μ_B) for all the samples was calculated using the relation given by Equation (7.4):

$$\mu_{eff}^{theo}(\mu_B) = \sqrt{0.6\mu_{eff}^2(Mn^{3+}) + (0.4 - x)\mu_{eff}^2(Mn^{4+})} \tag{7.4}$$

With $\mu_{eff}^{theo}(Mn^{3+}) = 4.9\ \mu_B$ and $\mu_{eff}^{theo}(Mn^{4+}) = 3.87\ \mu_B$ [Phong et al. (2016b)]. The value of $\mu_{eff}^{theo}(\mu_B)$ linearly decreases from 4.48 μ_B for x = 0.02 to 4.38 μ_B for x = 0.08. The value of experimental effective PM moment is greater than the value of theoretical

effective PM moment which could be due to the presence of FM fraction in PM state as discussed above. **Fig. 7.7**(b) demonstrates variation in experimental and theoretical values of effective PM moment as a function of Ti-doping concentration.

7.3.3.3. Griffiths Phase Analysis

For the sample LBMTO with x = 0.08, the inverse molar susceptibility χ_m^{-1} deviates downwardly below certain temperature in the PM regime similar to the results discussed in chapter 6. This sharp down-turn of χ_m^{-1} is characterized by Griffiths Phase (GP) which appears due to presence of FM ordering in PM regime. The other compositions do not exhibit Griffiths Phase behavior. As discussed earlier also, the onset temperature of sharp down-turn is defined as Griffiths' temperature (T_G). The inverse molar susceptibility, in the GP region ($T_C \leq T \leq T_G$) follows modified CW law given by Equation (7.5):

$$\chi_m^{-1} \propto (T - T_C^R)^{1-\lambda} \tag{7.5}$$

where, λ is exponent for magnetic susceptibility, lies in the range $0 \leq \lambda \leq 1$, which is a measure of deviation from CW law and T_C^R is critical temperature of random ferromagnet where susceptibility tend to diverge, lies below Griffiths' temperature T_G and above long-range ordering temperature T_C [Dayal et al. (2014)]. As detailed in chapter 6, the choice of T_C^R is very important for the correct determination of λ, characterizing the GP. Following the same procedure as in chapter 6, we choose $T_C^R = \theta_{CW} = 247.7$ K for x = 0.08. **Fig. 7.7(d)** presents a $\log_{10}\chi^{-1}$ vs. $\log_{10}(T/T_C^R - 1)$ plot for the dc susceptibility of the sample with x = 0.08 which exhibits linear portion in the high-temperature above T_G attributed to the PM regime. Fitting of this PM region with modified CW equation yielded $\lambda_{PM} = 0$. The fitting of χ_m^{-1} in the GP region provides $\lambda_{GP} = 0.95(1)$. A quite large value of λ_{GP} indicates the strength of GP in this system. A large range of obtained values for λ_{GP} is reported [Giri et al. (2014b]. However, the current

example demonstrates one of the robust GP scenario in manganites [Karmakar et al. (2012)], where the GP has been observed over a wide temperature range ~ 98 K (T_G - T_C).

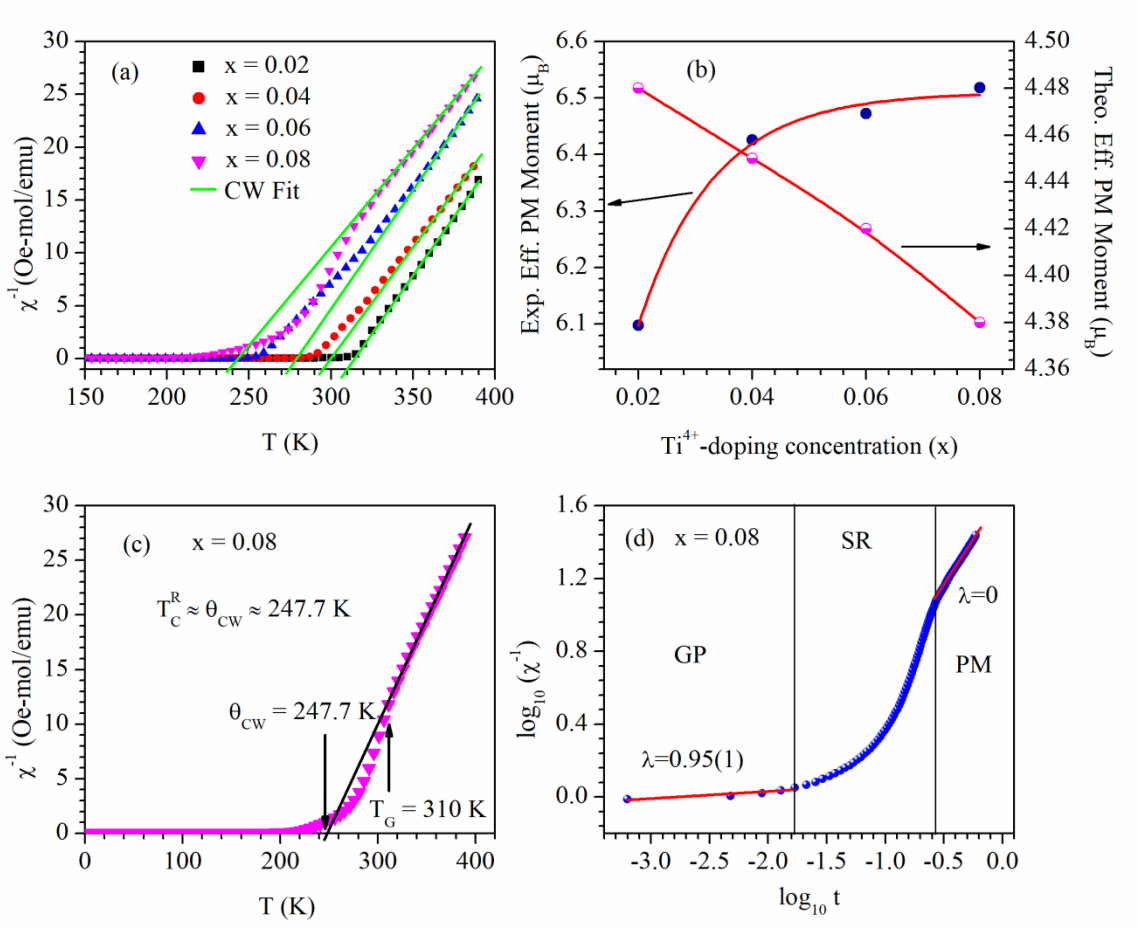

Figure 7.7: (a) Temperature dependence of inverse molar susceptibility (b) Variation of experimental and theoretical effective PM moments for LBMTO manganites with nominal compositions x = 0.02, 0.04, 0.06 and 0.08. (c) Inverse molar susceptibility for LBMTO with x = 0.08. (d) log-log plot between reduced temperature (t) and inverse molar susceptibility for LBMTO manganite with x = 0.08.

7.3.3.4. Field dependent Magnetization Studies

Figs. 7.8(a-b) demonstrates field dependence of magnetization M(H) plots of LBMTO manganites measured at 10K and 300 K in the magnetic field range -60 kOe to +60 kOe, respectively. The insets of **Fig. 7.8**(a-b) show low field zoomed view of

magnetic hysteresis loops, which clearly shows that all samples at 10 K are soft ferromagnets. We estimated values of remnant magnetization (M_r) and coercive field (H_C) for the magnetic hysteresis loops which are listed in **Table 3.3**. All the M(H) plots at 10 K increase sharply below 6 kOe and almost get saturation just above 10 kOe. The value of maximum magnetization say at 60 kOe decreases with increasing doping concentration of Ti^{4+}-ion showing dilution effect of the Ti^{4+}-ion and the decreases in the value of M(H) at 300 K is due to the PM contribution. The experimental saturation moment for the samples with x = 0.02, 0.04, 0.06 and 0.08 can be estimated from magnetization data measured at 10K and 300 K, separately, in the units of Bohr magneton per atomic formula unit using given Equation (7.6):

$$\mu_{sat}^{exp}\,(\mu_B/\mathrm{f.u.}) = M_{sat}^{exp}\,M_m/N_a\mu_B \tag{7.6}$$

Where, N_a is Avogadro's number, M_m the molecular mass, M_{sat}^{exp} the experimental value of saturation magnetization and μ_B the Bohr magneton. The experimental values of the saturation magnetization were determined by extrapolating straight line from higher-H to H = 0 as shown in **Fig. 7.3**(c). The experimental values of saturation moment at 300K are found to be 1.64, 1.31, 0.33 and 0.14 μ_B, whereas, the estimated values of saturation moment at 10 K are found to be 3.72, 3.74, 3.65 and 3.60 μ_B for LBMTO with x = 0.02, 0.04, 0.06 and 0.08, respectively. The value of μ_{sat}^{exp} can be compared with the theoretically calculated value of saturation moment, μ_{sat}^{theo} of "Mn" from its valence state taking into account the dilution effect of Ti^{4+}-ions.

If the spins of all Mn-ions are aligned in the same direction, then the magnetic moment of LBMTO manganites can be given by Equation (7.7):

$$\mu_{sat}^{theo}\,(\mu_B/\mathrm{f.u}) = 0.6M_{Mn^{3+}} + (0.4-x)M_{Mn^{3+}} + xM_{Ti^{4+}} \tag{7.7a}$$

$$\mu_{sat}^{theo}\,(\mu_B/\mathrm{f.u.}) = 2\mu_B\left[0.6\times\frac{4}{2} + (0.4-x)\times\frac{3}{2}\right] \tag{7.7b}$$

The theoretical values of spin only saturation moment were found to be 3.54, 3.48, 3.42 and 3.36 μ_B, respectively, which decreases with increasing doping concentration of non-magnetic Ti^{4+}-ion. The values of μ_{sat}^{exp} and μ_{sat}^{theo} were compared and found that experimental saturation moment μ_{sat}^{exp} at 10 K is greater than the spin only value of theoretical saturation moment μ_{sat}^{theo}, which suggests that at 10 K there is a contribution of orbital moment in saturation moment, i.e. spin-orbit coupling.

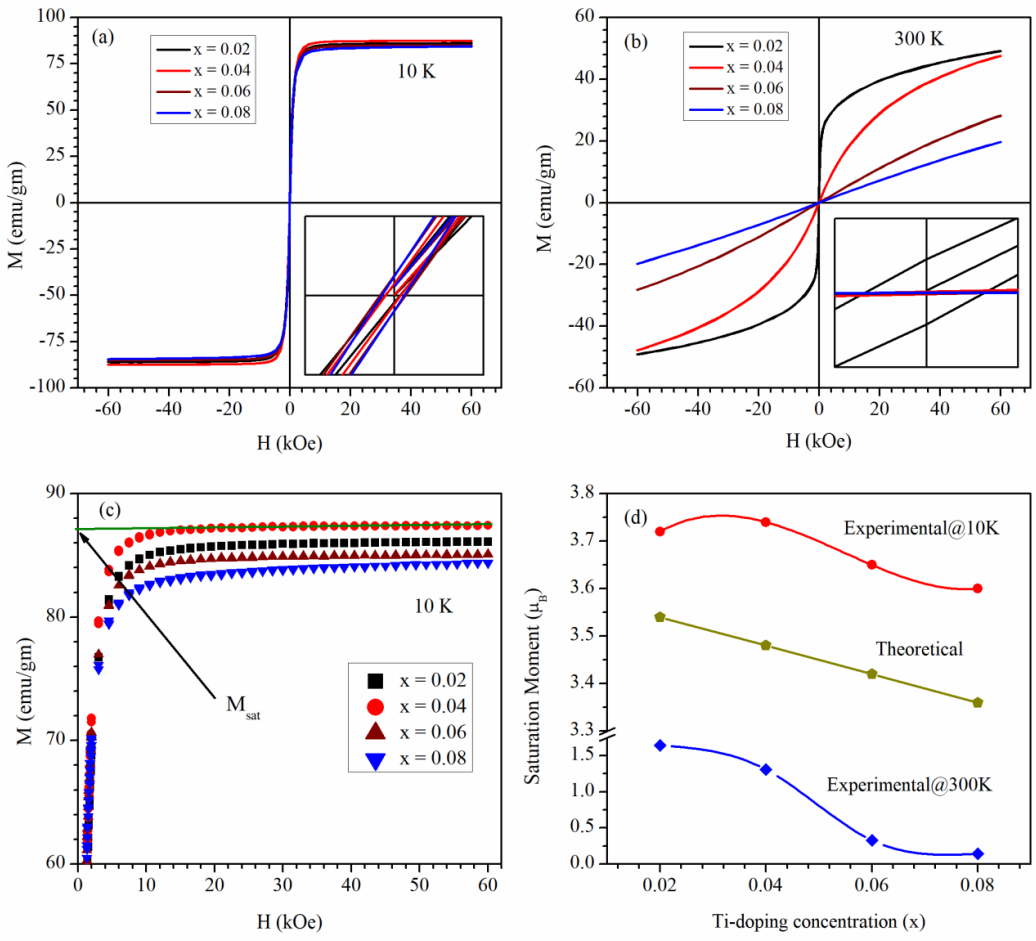

Figure 7.8: Field dependent magnetic hysteresis curves measured at (a) 10 K and (b) 300 K (c) Field dependent magnetization curves at 10 K (d) Variation of theoretical and experimental saturation moment as a function of Ti-doping concentration (x), for LBMTO manganites.

Table 7.3: The magnetic parameters for LBMTO manganites with x = 0.02, 0.04, 0.06 and 0.08. The Curie temperature T_C, Curie-Weiss temperature θ_{CW}, Curie constant C, the experimental effective paramagnetic moment μ_{eff}^{exp} (μ_B), the theoretical effective paramagnetic μ_{eff}^{theo} (μ_B), Remnant magnetization M_r, Coercive field H_C, experimental saturation moment μ_{sat}^{exp} (μ_B) and theoretical saturation moment μ_{sat}^{the} (μ_B).

x	**0.02**	**0.04**	**0.06**	**0.08**
T_C (K)	309	286	251	212
θ_{CW} (K)	313	294	264	246
C (emu.K/Oe.mol)	4.65	5.16	5.24	5.31
μ_{eff}^{exp} (μ_B)	6.10	6.42	6.47	6.52
μ_{eff}^{theo} (μ_B)	4.48	4.45	4.42	4.38
M_r @ 300 K (emu/gm)	2.22	0.09	0.02	0.02
M_r @ 10 K (emu/gm)	0.42	0.46	0.76	0.74
H_C @ 300 K (Oe)	31	32	33	26
H_C @ 10 K (Oe)	3	6	8	7
μ_{sat}^{exp} (μ_B/f.u.) @ 300 K	1.64	1.31	0.33	0.14
μ_{sat}^{exp} (μ_B/f.u.) @ 10 K	3.72	3.74	3.65	3.60
μ_{sat}^{theo} (μ_B/f.u.)	3.54	3.48	3.42	3.36

To further explore the nature of the magnetic phase transition, we studied isothermal Arrott's plot (M^2 vs. H/M). The nature of the magnetic phase transition in all the Ti-doped samples can be confirmed using the Banerjee criterion [Banerjee (1964)]. According to the Banerjee criterion, the magnetic transition is of second order if all the isothermal M^2 vs. H/M curves have a positive slope. Conversely, if some of the isothermal Arrott's curves show negative slope in some region, the transition is of first order [Ho et al. (2016); Banerjee (1964)]. **Fig. 7.9** shows Arrott's plots for LBMTO manganites. Insets of **Fig. 7.9** show zoomed view of Arrott's plots in the low value region of H/M. The slope of the Arrott's plots in higher field regions is positive, however, in low field region at some points slope is negative. This reveals that magnetic transition of LBMTO manganites is of first order in low field region and is of second

order in high field region. A similar behavior of magnetic transition was observed in Tb^{3+} doped $La_{0.5}Ca_{0.5}MnO_3$ manganite, which exhibits first order magnetic transition in the low field region, and switches to second order magnetic transition for the higher magnetic field above 10 T [Doshi et al. (2011)]. At high H/M values, the Arrott's plots are straight lines, which intersect M^2-axis (H = 0). These features indicate existence of long-range FM ordering. The intercept value of magnetization at H = 0 is known as spontaneous magnetization M_0 for ferromagnets. The value of M_0 decreases with increasing temperature. The values of M_0 at 10 K were found to be 85.54, 87.26, 85.05 and 83.86 emu/gm for x = 0.02, 0.04, 0.06 and 0.08, respectively, while, at 300 K, only x = 0.02 sample shows non-zero M_0 of 29.39 emu/gm.

7.3.3.5. Temperature dependent ac Susceptibility Studies

Fig. 7.10 displays temperature dependent ac susceptibility measured at 100, 300 and 500 Hz in the temperature range 2-390 K. In **Fig. 7.10**, left panel shows real part $\chi'(T)$ and right panel shows imaginary part $\chi''(T)$ of the ac susceptibility for LBMTO manganites. The qualitative behavior of the $\chi'(T)$ is similar to that of ZFC magnetization. The $\chi'(T)$ shows broad maxima peak near T_B, which is frequency independent. It shows two clear anomalies; one near T_B and other close to 8 K.

However, the qualitative behavior of $\chi''(T)$ for LBMTO samples is different from their respective $\chi'(T)$ and is similar to the $\chi''(T)$ for bulk sample of LBMO-40 manganite discussed in chapter 6. The $\chi''(T)$ curves of all samples exhibit a frequency independent sharp main peak close to T_{irr} along with several anomalies in the low temperature region. The corresponding characteristic is not obviously noticeable in the $\chi'(T)$ and this may happen as a result of the large real part of the susceptibility associated with ferromagnetism [Roy et al. (2008)]. The $\chi''(T)$ for the LBMTO manganites with x = 0.02, 0.04, 0.06 and 0.08 exhibit several anomalies in different

temperature regions, i.e., at T_{irr}, close to 190 K, near 49 K and at 8 K. In addition to this, the LBMTO manganite with x = 0.08 shows anomaly above T_{irr} at 285 K. The origin of these anomalies will be investigated in future.

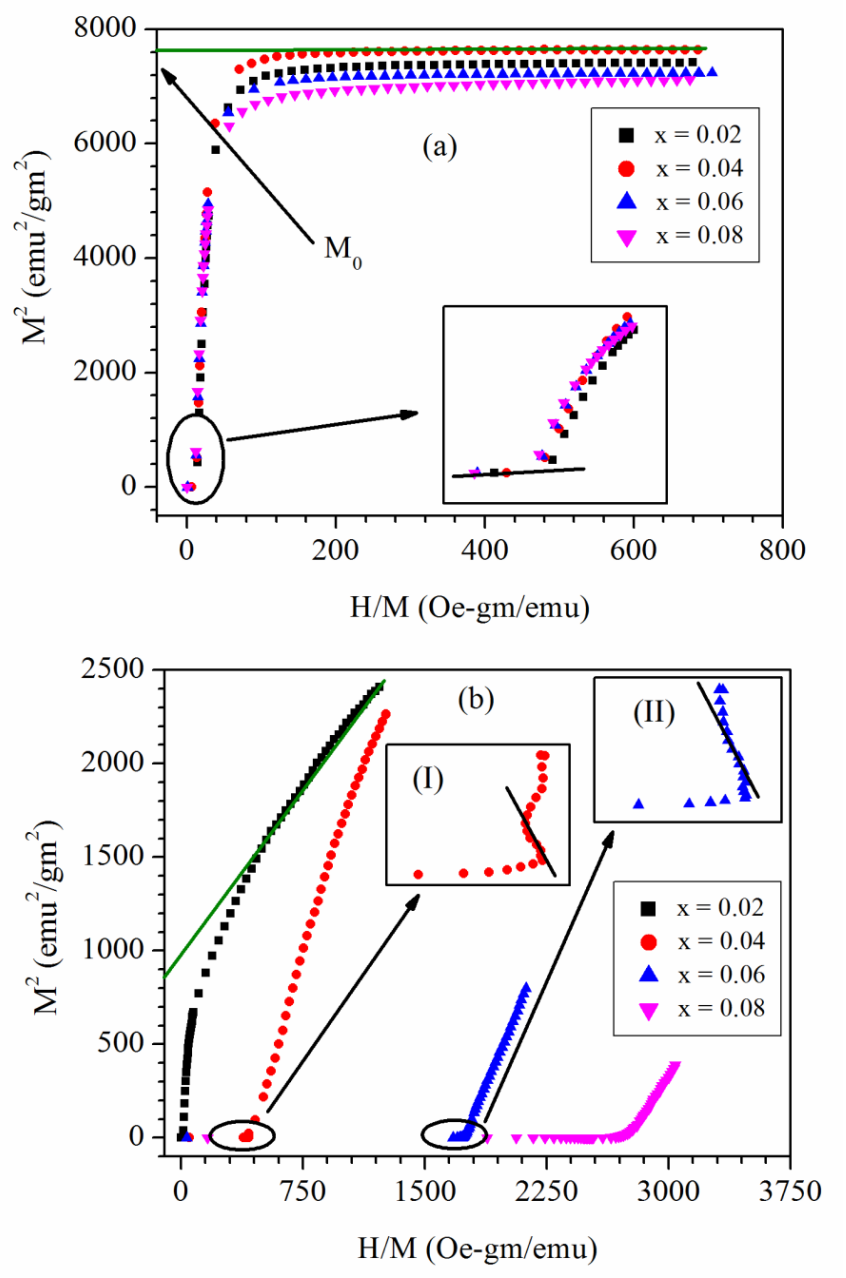

Figure 7.9: Arrott's plots M^2 versus H/M for LBMTO manganites measured at (a) 10 K and (b) 300 K. Inset of (a) shows zoomed view of Arrott's plots at 10 K. Insets (Ib) and (IIb) show zoomed view of Arrott's plots for $La_{0.6}Ba_{0.4}Mn_{1-x}Ti_xO_3$ manganites with x = 0.04 and 0.06.

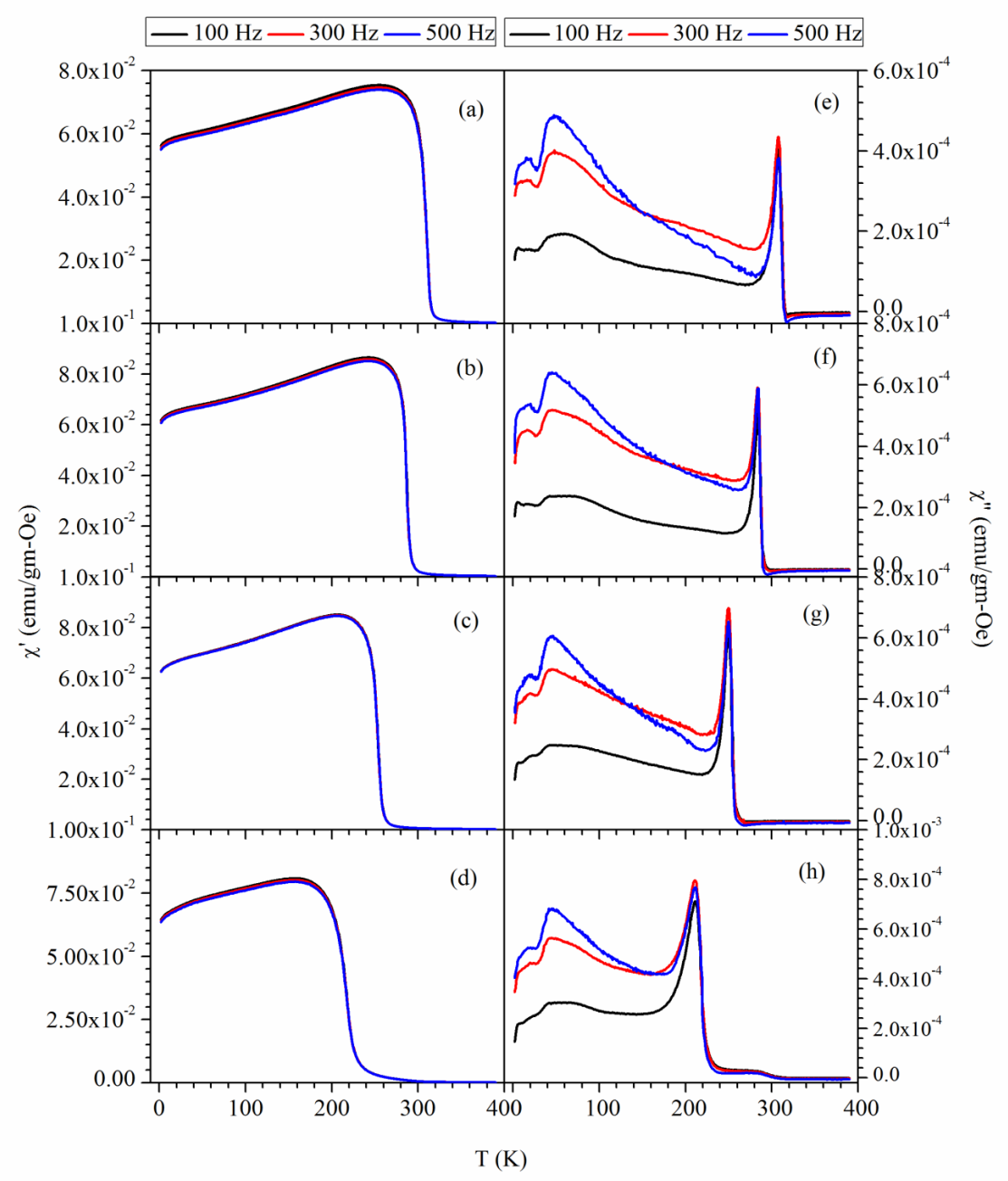

Figure 7.10: Temperature and frequency dependence of ac magnetic susceptibility real part (left panel) for $La_{0.6}Ba_{0.4}Mn_{1-x}Ti_xO_3$ manganites with x = (a) 0.02, (b) 0.04, (c) 0.06 and (d) 0.08 and imaginary part (right panel) for $La_{0.6}Ba_{0.4}Mn_{1-x}Ti_xO_3$ manganites with nominal compositions x = (e) 0.02, (f) 0.04, (g) 0.06 and (h) 0.08.

7.4. Conclusions

The polycrystalline samples of $La_{0.6}Ba_{0.4}Mn_{1-x}Ti_xO_3$ manganites with different compositions x = 0.02, 0.04, 0.06 and 0.08 were prepared using auto-combustion technique. Structural analysis was performed by Rietveld structural refinement of the XRD patterns for all the samples which reveals that LBMTO manganites crystallize into cubic structure having $Pm\bar{3}m$ space group. The lattice constant (a) and unit cell volume (V) increase with increasing concentration of Ti^{4+}-ion from a = 3.91182(5) Å to a = 3.91700(5) Å and V = 59.860(1) $Å^3$ to V = 60.098(1) $Å^3$ for changing Ti-content from 0.02 to 0.08, respectively due to replacement of Mn^{4+}-ions by Ti^{4+}-ions. The analysis of the SEM micrographs shows that particle size of the samples increases with increasing doping concentration of Ti^{4+}-ion. The temperature dependent magnetization study reveals that LBMTO manganites exhibit PM to FM magnetic phase transition and Curie temperature T_C decreases exponentially as a function of doping concentration of Ti^{4+}-ion from 309 K for x = 0.02 to 212 K for x = 0.08 due to weakening of DE interaction. The effective experimental value of PM moment increases exponentially from 6.10 μ_B for x = 0.02 to 6.52 μ_B for x = 0.08 due to presence of FM state in PM region. Downturn deviation of inverse susceptibility from CW law for the sample with x = 0.08 reveals the signature of Griffiths phase. The singularity of the dc inverse susceptibility in Griffiths phase region provides the numerical values of Griffiths temperature (T_G), critical temperature for random ferromagnet (T_C^R) and the exponent (λ_{GP}) to be 310 K, 247.7 K and 0.95(1), respectively. The irreversibility between zero field cooled and field cooled magnetization reveals spin glass cluster behavior of the samples due to the inhomogeneity of magnetic ordering. The temperature and frequency dependent ac susceptibility measurements show several anomalies and needs to be understood properly.